Journal of Solid State Chemistry 184 (2011) 2428–2433

Contents lists available at ScienceDirect

Journal of Solid State Chemistry

journal homepage: www.elsevier.com/locate/jssc

Structural and magnetic characterization of $BiFe_xMn_{2-x}O_5$ oxides ($x=0.5$, 1.0)

M. Retuerto [a,b,*], M.J. Martínez-Lope [a], K. Krezhov [c], M.T. Fernández-Díaz [d], J.A. Alonso [a]

[a] Instituto de Ciencia de Materiales de Madrid, C.S.I.C., Cantoblanco, E-28049 Madrid, Spain
[b] Department of Chemistry and Chemical Biology, Rutgers, The State University of New Jersey, 610 Taylor Road Piscataway, NJ 08854-808, USA
[c] Institute for Nuclear Research and Nuclear Energy, Bulgarian Academy of Sciences, 72 Tsarigradsko Chaussee Boulevard, Sofia 1784, Bulgaria
[d] Institut Laue-Langevin, BP156X, Grenoble F-38042, France

ARTICLE INFO

Article history:
Received 14 February 2011
Received in revised form
6 July 2011
Accepted 7 July 2011
Available online 18 July 2011

Keywords:
RMn_2O_5
$BiMn_2O_5$
Multiferroic oxides
Magnetoelectric
Ferromagnetic
Neutron diffraction

ABSTRACT

The title compounds have been synthesized by a citrate technique followed by thermal treatments in air ($BiFe_{0.5}Mn_{1.5}O_5$) or under high oxygen pressure conditions ($BiFeMnO_5$), and characterized by X-ray diffraction (XRD), neutron powder diffraction (NPD) and magnetization measurements. The crystal structures have been refined from NPD data in the space group *Pbam* at 295 K. These phases are isostructural with RMn_2O_5 oxides (R=rare earths) and contain infinite chains of $Mn^{4+}O_6$ octahedra sharing edges, linked together by $(Fe,Mn)^{3+}O_5$ pyramids and BiO_8 units. These units are strongly distorted with respect to those observed in other $RFeMnO_5$ compounds, due to the presence of the electronic lone pair on Bi^{3+}. It is noteworthy the certain level of antisite disorder exhibited in both samples, where the octahedral positions are partially occupied by Fe cations, and vice versa. $BiFe_xMn_{2-x}O_5$ ($x=0.5$, 1.0) are short-range magnetically ordered below 20 K for $x=0.5$ and at 40 K for $x=1.0$. The main magnetic interactions seem to be antiferromagnetic (AFM); however, the presence of a small hysteresis in the magnetization cycles indicates the presence of some weak ferromagnetic (FM) interactions.

1. Introduction

The systems that simultaneously combine magnetism and ferroelectricity are very attractive from a technological point of view due to the possibility of controlling the dielectric properties using an external magnetic field [1,2]. Unfortunately, materials showing large magnetoelectric effects (ME) are extremely rare. RMn_2O_5 (R=rare earths) compounds are among the few oxides showing a significant ME, thus numerous current investigations are focused on the study of these materials [3–7].

The RMn_2O_5 family of oxides was first described in the 1960s by Quezel-Ambrunaz et al. [8] and Bertaut et al. [9] in single crystal form prepared from a Bi_2O_3 flux and they determined the structural parameters of the complete series. The crystal structure of RMn_2O_5 (orthorhombic, space group *Pbam*) is attractive because it contains two crystallographically independent sites for Mn atoms, with different oxygen coordination and oxidation states [10,11]: Mn^{4+} ions are located at the 4*f* sites, octahedrally coordinated to oxygen atoms, whereas Mn^{3+} ions occupy the 4*h* sites and they are bonded to five oxygen atoms, forming a distorted tetragonal pyramid. The structure contains infinite chains of edge-sharing $Mn^{4+}O_6$ octahedra, running along the *c*-axis, and the different chains are interconnected by the $Mn^{3+}O_5$ pyramids and RO_8 scalenohedra.

With the aim to induce novel magnetic and ferroelectric properties in the RMn_2O_5 series, we have recently designed and prepared the family of oxides of formula $RFeMnO_5$ (R=Y, Tb, Dy, Ho, Er, Yb) [12–17], which are obtained by replacing Mn^{+3} by Fe^{3+}. In this paper we report on the preparation of two compounds of stoichiometry $BiFe_xMn_{2-x}O_5$ ($x=0.5$, 1.0), which are isostructural with $BiMn_2O_5$ [18]. These oxides have been synthesized from a citrate-precursors procedure followed by annealing under high-O_2 pressure for $x=1.0$, and the products have been characterized from the structural point of view from NPD. This study was completed with macroscopic magnetic susceptibility measurements.

Previous work concerning this system refers to the solid solution $Bi_2Fe_{4-x}Mn_xO_{9+d}$ reported by Masuno [19] and Jiménez [20]. Masuno [19] reported that it only exists a limited miscibility on either sides of the phase diagram, where $0 \le x \le 0.9$ and $3.6 \le x \le 4.0$, while for $0.9 < x < 3.6$ there is a multiphase region containing $Bi_2Fe_4O_9$, $Bi_2Mn_4O_{10}$ ($BiMn_2O_5$) and the perovskite $Bi(Fe,Mn)O_3$. According to Jiménez [20], a complete solid solution exists in the entire range of x; however, it was assumed that the two end members were actually isostructural and therefore that their X-ray powder diffraction patterns were identical. This assumption could not be possible since, upon altering the oxygen content, both the structure and the powder patterns have to

* Corresponding author at: Department of Chemistry and Chemical Biology, Rutgers, The State University of New Jersey, 610 Taylor Road Piscataway, NJ 08854-808, USA.
E-mail address: retuerto@rci.rutgers.edu (M. Retuerto).

0022-4596/$ - see front matter © 2011 Elsevier Inc. All rights reserved.
doi:10.1016/j.jssc.2011.07.009

change noticeably. Afterwards, Giaquinta and zur Loye [21] presented the synthesis and the structure of $Bi_2Fe_2Mn_2O_{10}$ ($BiFeMnO_5$) determined by single-crystal X-ray diffraction. They found that the iron and manganese ions were ordered in the octahedral and square pyramidal sites, respectively. Our results, based upon a high-resolution neutron powder diffraction investigation, suggest an opposite occupation of Fe and Mn cations.

2. Experimental

$BiFe_xMn_{2-x}O_5$ ($x=0.5$, 1.0) were obtained as black-colored polycrystalline powders by a chemical route using citrates as precursors. Stoichiometric amounts of analytical grade Bi_2O_3, $FeC_2O_4.2\,H_2O$ and $MnCO_3$ were dissolved in citric acid. The citrate solution was slowly evaporated, leading to organic resins containing a random distribution of the involved cations at an atomic level. These resins were first dried at 120 °C. The samples were then heated at 600 °C for 12 h in order to eliminate all the organic materials. For $x=0.5$ the precursors were treated at 800 °C during 15 h in air and for $x=1.0$ the precursors were slowly heated up to 825 °C at a final pressure of 100 bar of O_2 in a VAS furnace, and held at this temperature for 10 h. About 2 g of the precursor powders were contained in a gold can during the oxygenation process. The product was finally cooled, under pressure, at 300 °C h^{-1} down to room temperature. Finally, the oxygen pressure was slowly released.

The initial characterization of the products was carried out by laboratory X-ray diffraction (XRD) (Cu$K\alpha$, $\lambda=1.5406$ Å). Neutron powder diffraction (NPD) diagrams were collected at the Institut Laue-Langevin (ILL) in Grenoble (France). The crystallographic structures were refined from high-resolution NPD patterns acquired at room temperature (RT) at the D2B diffractometer with $\lambda=1.594$ Å for $BiFe_{0.5}Mn_{1.5}O_5$ ($x=0.5$) and D1A diffractometer with $\lambda=1.910$ Å for $BiFeMnO_5$ ($x=1.0$). Low temperature NPD data were collected at the D20 diffractometer (ILL) with $\lambda=2.42$ Å, in the temperature range 3–170 K. The refinement of the crystal structures was performed by the Rietveld method [22], using the FULLPROF refinement program [23]. A pseudo-Voigt function was chosen to generate the line shape of the diffraction peaks. The following parameters were refined in the final runs: scale factor, background coefficients, zero-point error, pseudo-Voigt corrected for asymmetry parameters, positional coordinates and isotropic thermal factors. The coherent scattering lengths for Bi, Fe, Mn and O are 0.8532, 9.45, −3.73 and 5.805 fm, respectively.

The magnetic measurements were performed in a commercial superconducting quantum interference device magnetometer (SQUID). The *dc* susceptibility was measured under a 0.1 T magnetic field in the temperature interval $2<T<400$ K. Isothermal magnetization curves were obtained for magnetic fields going from −5 to 5 T at $T=5$ K.

3. Results

$BiFe_xMn_{2-x}O_5$ ($x=0.5$, 1.0) samples were obtained as well-crystallized polycrystalline powders. Fig. 1 shows the XRD patterns of $BiFe_xMn_{2-x}O_5$ ($x=0.5$, 1.0) together with that of $BiMn_2O_5$ ($x=0.0$) for the sake of comparison. They correspond to pure phases that can be indexed in orthorhombic unit cells isotopic to RMn_2O_5, with no additional peaks that could indicate the presence of impurities, superstructures or departure of the mentioned symmetry.

3.1. Crystallographic structure

The refinement of the crystallographic structures has been carried out from the NPD patterns acquired at RT in the space group *Pbam*, taking as the starting structural model that of $BiMn_2O_5$ [18]. Bi atoms

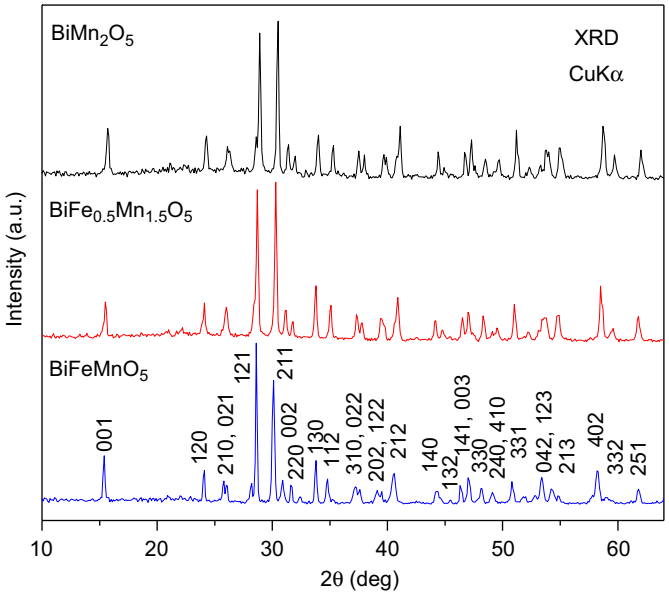

Fig. 1. XRD patterns for $BiMn_{2-x}Fe_xO_5$ ($x=0$, 0.5, 1.0) collected with Cu$K\alpha$ radiation. $BiFe_{0.5}Mn_{1.5}O_5$ and $BiFeMnO_5$ are indexed in an orthorhombic unit cell with $a=7.6165(6)$, $b=8.5352(5)$ and $c=5.8201(4)$ Å.

were located at 4*g* (*x y* 0) positions, Mn at 4*f* (0 ½ *z*) sites, Fe at 4*h* (*x y* ½) and the four crystallographically independent oxygen atoms at 4*e* (0 0 *z*), 4*g*, 4*h* and 8*i* (*x y z*) positions. A good agreement between the calculated and the observed patterns of $BiFe_xMn_{2-x}O_5$ ($x=0.5$, 1.0) after the Rietveld refinement is displayed in Fig. 2. The main structural parameters obtained after the fit are listed in Table 1. Neutrons are well suited to distinguish between Fe and Mn, thanks to the contrasting scattering lengths of these elements; the preferential location of Fe at the pyramidal sites and Mn in octahedral coordination is certain, but with a significant level of antisite disorder between Fe and Mn cations. For $x=0.5$, 3.6(8)% of the 4*f* Mn positions are occupied by Fe cations, whereas the 4*h* sites are occupied at 46.4(4)% by Fe and 53.6(4)% by Mn. For $x=1.0$, the degree of disorder is 24.2(4)%, as it is shown in Table 1. A selection of the most important atomic distances and angles is listed in Table 2. It is plausible to consider that antisite Fe at the octahedral positions is Fe^{4+}. This assumption is based on the fact that $BiFeMnO_5$ (showing the largest antisite effect) was prepared under high O_2 pressure (100 bar), and in these conditions Fe^{4+} can be stabilized in octahedral coordination; for instance $CaFeO_3$ can be prepared under O_2 pressure starting from citrate precursors [24]. A second possibility is that the electroneutrality is preserved if some Mn^{4+} is introduced on the pyramidal sites as Fe^{3+} occupies the octahedral sites, probably the actual situation is intermediate between both hypotheses.

A view of the crystallographic structure is displayed in Fig. 3. There are two different oxygen environments for the atoms that occupy the 4*f* and 4*h* sites. At the 4*f* site, the Mn^{4+} ions are inside of $Mn^{4+}O_6$ distorted octahedra, whereas at the 4*h* site, the Mn^{3+} ions form $Fe^{3+}O_5$ square pyramids (disregarding the antisite effect). The pyramids share edges to form Fe_2O_{10} dimer units, linked via O1 oxygen atoms. The structure contains infinite chains of $Mn^{4+}O_6$ octahedra sharing edges via O2 and O3 oxygens, running along the *c*-axis. The different chains of $Mn^{4+}O_6$ are interconnected through the Fe_2O_{10} pyramidal dimer units via O3 and O4 oxygen atoms (Fig. 3).

3.2. Magnetic measurements

The susceptibility vs. temperature data of $BiFe_xMn_{2-x}O_5$ ($x=0.5$, 1.0) are shown in Fig. 4. At low temperature, the

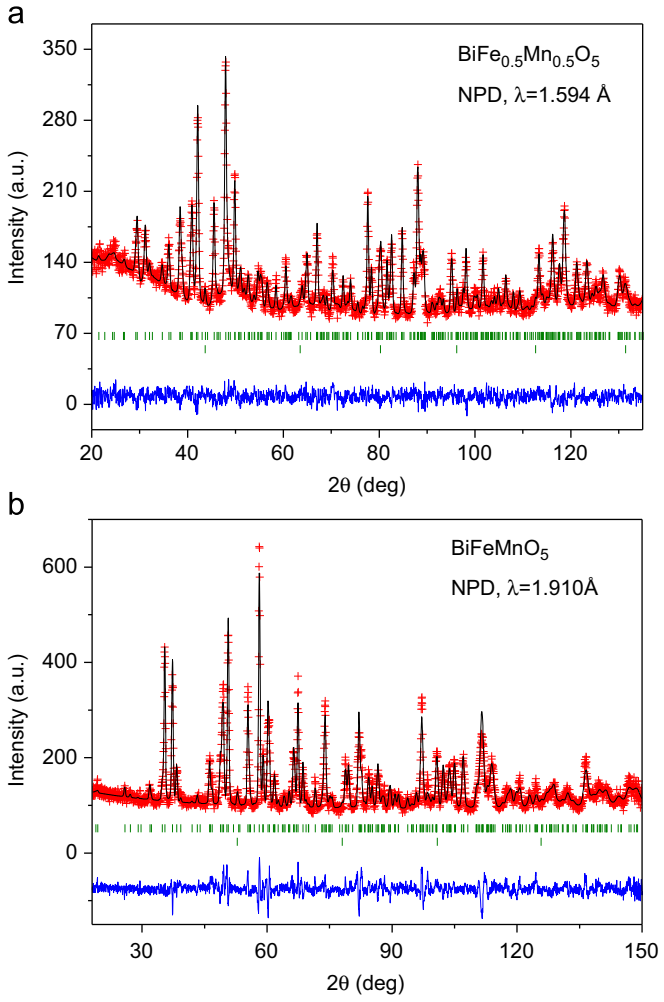

Fig. 2. Comparison of the observed (crosses), calculated (solid line) and difference (at the bottom) NPD patterns at room temperature. The tick marks correspond to the position of the allowed Bragg reflections for (a) $BiFe_{0.5}Mn_{1.5}O_5$ and (b) $BiFeMnO_5$. The second line of tick marks correspond to vanadium from the sample holder.

susceptibility of both samples increases and exhibits a broad maximum at $T_N=20$ K for $x=0.5$ and at 40 K for $x=1.0$. This peak suggests the appearance of some kind of magnetic ordering in both samples. For $x=0.5$ there is a divergence between ZFC (zero-field cooled) and FC (field cooled) curves. Both curves only diverge at low temperatures, immediately below T_N, whereas the FC susceptibility remains almost invariable, and the ZFC curve presents a decay of the susceptibility upon cooling.

Fig. 4 also shows the inverse of the susceptibility curves for both samples. These curves appear to indicate a non-Curie–Weiss type behavior even at very high temperatures, indicating the existence of short-range magnetic order above T_C or some kind of frustration. The fact that the slope in the $x=1$ sample changes so abruptly at ~375 K could indicate a possible magnetic impurity or other interesting magnetic interactions at high temperatures.

The magnetization vs. magnetic field curves at $T=5$ K for both samples ($x=0.5$ and 1.0) are illustrated in Fig. 5. They are almost linear. This behavior is reminiscent of antiferromagnetic systems such as $BiMn_2O_5$ [18]. However, both samples exhibit a very small hysteresis at $T=5$ K, indicating the presence of weak ferromagnetic interactions.

Low temperature NPD data are shown in Fig. 6; no additional contribution to the scattering that may come from the long-distance ordering of the Mn or Fe spins is observed as the sample is cooled from 170 to 3 K. This observation suggests the presence of short range magnetic ordering or some kind of frustration, perhaps related with the antisite disordering observed in both samples.

Table 1
Unit-cell, positional, thermal parameters and occupancies of $BiFe_xMn_{2-x}O_5$ ($x=0.5$, 1.0) refined in the orthorhombic *Pbam* (No. 55) space group, $Z=4$, from NPD data at 295 K. Bi and O2 atoms are at 4*g*(*x*,*y*,0) positions; (Mn,Fe)1 at 4*f*(0,½,*z*); (Fe,Mn)2 and O3 at 4*h*(*x*,*y*,½); O1 at 4*e*(0,0,*z*) and O4 at 8*i*(*x*,*y*,*z*) positions. Reliability factors are also given.

x	0.5	1.0
a (Å)	7.5635(5)	7.6165(6)
b (Å)	8.5598(5)	8.5352(5)
c (Å)	5.7738(3)	5.8201(4)
V (Å^3)	373.81(4)	378.36(4)
Bi		
x	0.1572(7)	0.1572(6)
y	0.1644(6)	0.1646(5)
B_{iso} (Å^2)	0.4(1)	0.81(6)
(Mn/Fe)1		
z	0.255(3)	0.265
$f_{occup.}$	0.964(4)/0.036(4)	0.758(4)/0.242(4)
B_{iso} (Å^2)	1.1(3)	0.3
(Fe/Mn)2		
x	0.3866	0.3721(8)
y	0.3478	0.3453(8)
$f_{occup.}$	0.964(4)/0.036(4)	0.758(4)/0.242(4)
B_{iso} (Å^2)	0.89	0.95
O1		
z	0.280(1)	0.294(2)
B_{iso} (Å^2)	0.83	1.2(1)
O2		
x	0.157(1)	0.154(1)
y	0.4437(8)	0.438(8)
B_{iso} (Å^2)	0.6(1)	1.20(8)
O3		
x	0.144(1)	0.141(1)
y	0.4277(9)	0.4184(7)
B_{iso} (Å^2)	0.8(1)	0.72(8)
O4		
x	0.3861(5)	0.3834(6)
y	0.1977(7)	0.1971(6)
z	0.253589)	0.2494(7)
B_{iso} (Å^2)	0.56(9)	1.26(8)
Reliability factors		
χ^2	1.10	2.40
R_p (%)	3.35	6.19
R_{wp} (%)	4.19	7.86
R_{exp} (%)	3.99	5.07
R_I (%)	7.81	8.49

4. Discussion

The crystal structure of $BiFe_xMn_{2-x}O_5$ ($x=0.5$, 1.0) is tightly related to that of $BiMn_2O_5$ ($x=0$) oxide (containing one Mn^{3+} and one Mn^{4+} cation per formula) by replacement of Mn^{3+} by Fe^{3+} cations in the square-pyramidal units. However some distinct features have been found in the structural parameters and in the bonding distances when Fe is introduced in the structure. Despite the fact that the ionic radii of Fe^{3+} and Mn^{3+} cations are very similar (0.645 Å in six-fold coordination and high-spin state [25]), the substitution of the Mn^{3+} cations by Fe^{3+} gives rise to an expansion of the unit-cell parameters from $x=0$ ($a=7.56078(8)$ Å, $b=8.53299(8)$ Å, $c=5.76066(5)$ Å and $V=371.654(6)$ Å^3) [18] to $x=0.5$ and finally to $x=1.0$ (Table 1). This expansion upon Mn

Table 2
Main interatomic distances (Å) and angles (deg.) for the $BiFe_xMn_{2-x}O_5$ (x=0, 0.5, 1.0) series.

x	0[a]	0.5	1.0
$R^{3+}O_8$ bicapped prism			
Bi–O1(× 2)	2.488(1)	2.451(7)	2.517(8)
Bi–O2	2.374(2)	2.391(9)	2.335(8)
Bi–O2	2.353(2)	2.354(10)	2.407(9)
Bi–O4(× 2)	2.267(2)	2.286(6)	2.270(6)
Bi–O4(× 2)	2.785(2)	2.782(6)	2.802(6)
〈Bi–O〉	2.476(2)	2.473(7)	2.490(7)
$(Mn, Fe)^{4+}O_6$ octahedra			
(Mn, Fe)1–O2(× 2)	1.968(2)	1.953(14)	1.999(5)
(Mn, Fe)1–O3(× 2)	1.870(2)	1.890(14)	1.884(5)
(Mn, Fe)1–O4(× 2)	1.916(2)	1.899(6)	1.904(5)
<(Mn, Fe)1–O>	1.916(2)	1.914(11)	1.929(5)
$(Fe,Mn)^{3+}O_5$ tetragonal pyramids			
(Fe,Mn)2–O1(× 2)	1.899(2)	2.011(7)	2.032(8)
(Fe,Mn)2–O3	2.085(3)	1.958(9)	1.867(10)
(Fe,Mn)2–O4(× 2)	1.929(2)	1.918(6)	1.933(6)
<(Fe,Mn)2–O>	1.948(3)	1.963(7)	1.959(8)
Mn–Mn	2.751(4)	2.94(2)	3.0557(2)
Mn–Mn	3.010(4)	2.83(2)	2.7644(2)
Fe–Fe	2.894(3)	3.1185(1)	3.282(9)
Fe–O1–Fe	99.3(2)	101.7(2)	107.7(5)
Mn–O2–Mn	99.8(2)	97.8(12)	99.7(2)
Mn–O3–Mn	94.7(2)	96.9(13)	94.4(2)
Mn–O3–Fe	131.2(2)	130.9(6)	131.4(5)
Mn–O4–Fe	123.0(1)	126.4(5)	124.7(4)

[a] Taken from Ref. [18].

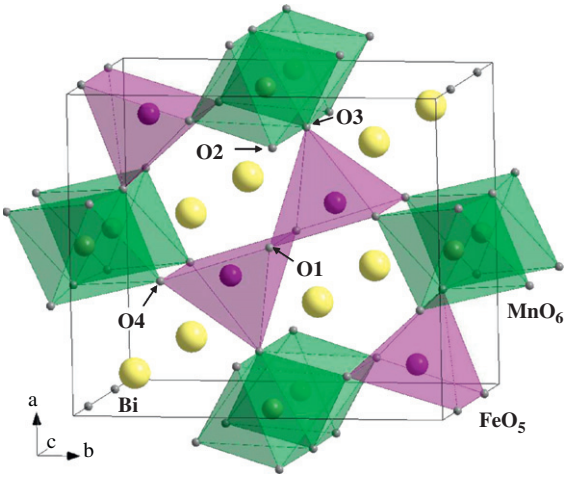

Fig. 3. A view of the crystallographic structure of $BiFeMnO_5$, approximately along the c-axis. Octahedra and tetragonal pyramids correspond to $Mn^{4+}O_6$ and $Fe^{3+}O_5$ polyhedra, respectively. Octahedra share edges, forming infinite chains along the c-axis. Pyramids form dimer units, linking together the chains of octahedra. Spheres represent the Bi atoms.

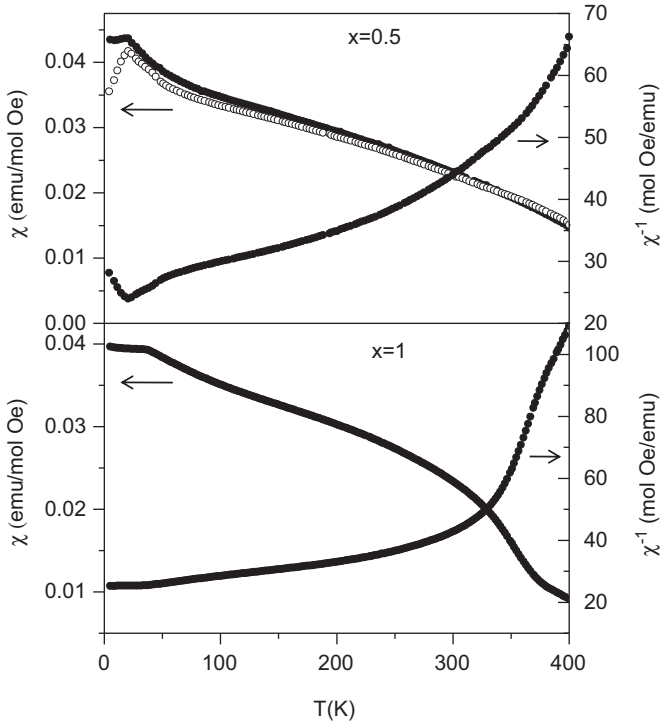

Fig. 4. Temperature dependence of the field cooling (FC) and zero field cooling (ZFC) dc susceptibility for $BiFe_xMn_{2-x}O_5$ (x=0.5, 1.0). Right axis: thermal evolution of the inverse of the susceptibility (ZFC data).

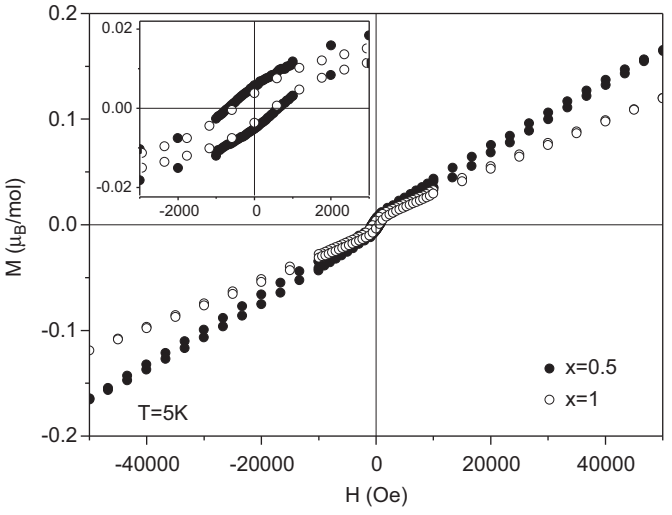

Fig. 5. Magnetization vs. magnetic field isotherms at T=5 K for $BiFe_xMn_{2-x}O_5$ (x=0.5, 1.0). The inset shows the low field region of the isotherms.

replacement by Fe has been observed in other RMnFeO$_5$ with respect to the respective parent RMn$_2$O$_5$ oxides, e.g. for R=Dy [14] or Ho [15] or Er [16]. This expansion could be related to the disorder between Mn and Fe cations over 4f and 4h sites, due to the replacement of some Mn^{4+} by Fe^{4+} cations in the octahedral sites. In this case, the Fe^{4+} size (0.585 Å) is substantially bigger than the ionic radii of Mn^{4+} (0.53 Å) in six-fold coordination. If we suppose that some Fe^{3+} is introduced at the octahedral sites, its bigger radii (0.645 Å) also could explain the increment of the unit-cell parameters. In fact this expansion is more pronounced from x=0.5 to 1.0 than from x=0 to 0.5, which is concomitant with the much higher disorder found in x=1.0 (24.2(4)%) than in x=0.5 (3.6(4)%) oxides.

The effect of Fe introduction is also noteworthy in the bonding distances of the $Mn^{4+}O_6$, $(Mn,Fe)^{3+}O_5$ and $Bi^{3+}O_8$ polyhedra. As discussed before, in the MnO_6 octahedra the average distances slightly increase due to the introduction of Fe^{4+} or Fe^{3+} ions (Table 2). Additionally, the Mn–Mn distances within the chains of octahedra (running along c-axis) strongly vary in the series, from 2.751/3.104 Å in $BiMn_2O_5$ to 3.055/2.764 Å in $BiFeMnO_5$. These distances have a paramount importance in determining the sign of the magnetic coupling along the chains, being FM and AFM for the shortest and longest Mn–Mn distances in $BiMn_2O_5$ [18], respectively. Regarding the $(Mn,Fe)O_5$ tetragonal pyramids, when x increases the square-pyramidal units become more flattened. The replacement of Mn^{3+} by Fe^{3+} originates a substantial shortening of the axial bonding distance ((Fe,Mn)–O3), from 2.085 Å (x=0) to

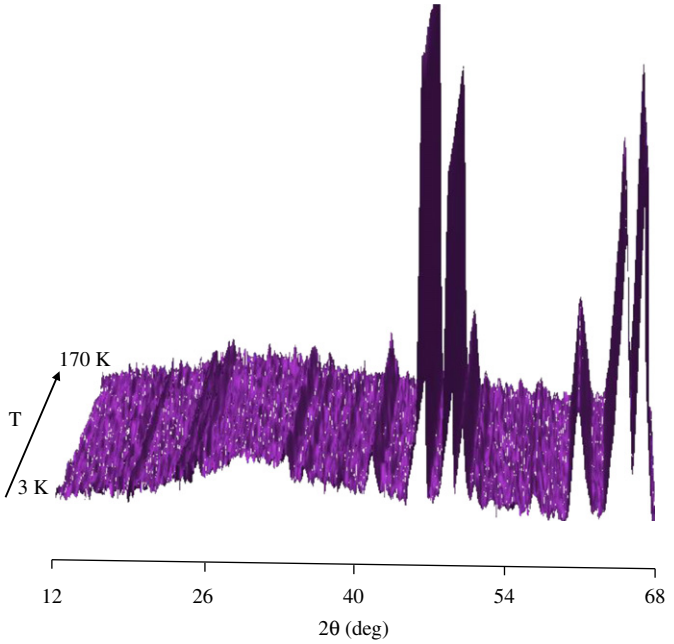

Fig. 6. Low temperature NPD data, collected in the 3–170 K range with λ=2.42 Å.

1.867 Å (x=1.0), and an enlargement of the equatorial bonding distances (Fe,Mn)–O4 and (Fe,Mn)–O1, with a slight average expansion of the pyramidal units. The changes observed in the bonding distances within the square pyramids cannot be related to the ionic radii, since Mn^{3+} and Fe^{3+} exhibit the same tabulated value [25]; this expansion is very probably correlated to the Jahn–Teller character of Mn^{3+} cations, favoring an increase of the axial bond-lengths in the $Mn^{3+}O_5$ pyramids, in contrast with the non-Jahn–Teller character of Fe^{3+} ($3d^5$ configuration).

As shown in Fig. 3, every two $Fe^{3+}O_5$ pyramids, doubly linked by O1 oxygens, form a dimer unit Fe_2O_{10}. Four $Mn^{4+}O_6$ octahedra chains are linked by a dimer unit through O3 and O4 oxygens. With respect to the parent $BiMn_2O_5$ oxide, it is also remarkable that the M–M (M=Fe, Mn) distances between square pyramids (within the dimer units) noticeably increases from 2.894 Å ($BiMn_2O_5$ [18]) to 3.118 Å ($BiMn_{1.5}Fe_{0.5}O_5$) to 3.282 Å ($BiMnFeO_5$). It seems that the replacement of Mn^{3+} by Fe^{3+} leads these cations to shift towards the pyramid apex; this shift is responsible for the observed increase of the Fe–Fe distances. This shift has already being observed in other RMnFeO$_5$ oxides, for instance ErMnFeO$_5$ [16] where Fe–Fe within the dimer is 2.956 Å, compared to Mn–Mn in $ErMn_2O_5$, of only 2.843(7) Å. In our present case, this shift is considerably more important, and it certainly drives a weakening of the Fe–Fe magnetic interactions within the dimer, whereas ErFeMnO$_5$ or YFeMnO$_5$ experiences a clear FM ordering at T_C=165 K [16,12], where the intra-dimer FM coupling plays an important role [12], in $BiMnFeO_5$ the magnetic interactions do not lead to the establishment of a long-range ferrimagnetic ordered structure, as also confirmed from low temperature NPD data (Fig. 6).

With respect to the oxygen coordination of Bi^{3+} cations, it can be described as $Bi^{3+}O_8$ bicapped prisms, with average ⟨Bi–O⟩ distances of 2.490 Å for x=1.0, slightly bigger than the ⟨Bi–O⟩ bond lengths of 2.476 Å observed in $BiMn_2O_5$. It is worth mentioning that Bi polyhedra are significantly more distorted in these compounds than the RO_8 units in other RFeMnO$_5$ oxides. A coupled shift of the Bi position along the [110] direction is observed with respect to the position of the rare-earth cations. As a consequence, the two Bi–O4 distances in BiFeMnO$_5$ are much shorter (2.270 Å) or longer (2.802 Å), respectively, than the corresponding other R members. For instance, in DyFeMnO$_5$ the Dy–O4 bond lengths are 2.354(6) and 2.465(6) Å, respectively [14], and in HoFeMnO$_5$, Ho–O4 bond lengths are 2.348(4) and 2.471(4) Å, respectively [15]. The distortion of this coordination environment is as a result of the presence of the electron lone pair on Bi^{3+}. The repulsion of the lone pair leads to an asymmetric distribution of the Bi–O bonds, involving significant shifts of some oxygen positions.

Regarding the magnetic properties, it seems that the main magnetic interactions are antiferromagnetic, like those observed in $BiMn_2O_5$ [18], where different ferromagnetic and antiferromagnetic superexchange interactions between Mn^{4+}–Mn^{4+}, Mn^{4+}–Mn^{3+} and Mn^{3+}–Mn^{3+} cations in the different positions are competing to generate a global antiferromagnetic structure. However, the presence of a small hysteresis in the magnetization isotherms of $BiFe_xMn_{2-x}O_5$ (x=0.5, 1.0) indicates the presence of some weak ferromagnetic interactions. This is in strong contrast with all the members of the RFeMnO$_5$ series (R=rare earths), which exhibit ferrimagnetic structures. In RFeMnO$_5$, the magnetic ordering of the Mn^{4+} and Fe^{3+} sublattices is defined by the interactions that appear between the Mn^{4+}–Mn^{4+}, Mn^{4+}–Fe^{3+} and Fe^{3+}–Fe^{3+} cations. The magnetic moments between Mn^{4+} and Mn^{4+} in the octahedral sites as well as the moments within the Fe^{3+}–Fe^{3+} dimers in the pyramidal positions are ferromagnetically coupled, and both Mn^{4+}–Fe^{3+} sublattices are antiferromagnetically coupled in a global ferrimagnetic structure.

In the $BiFe_xMn_{2-x}O_5$ (x=0.5, 1.0) samples we observe a global antiferromagnetic behavior (over-imposed with a weak ferromagnetism effect) driven by three factors: (i) the antisite disordering observed between Mn and Fe sublattices, specially important for BiFeMnO$_5$ (24.2% compared to 4.6% for ErFeMnO$_5$ [16]); (ii) the extraordinary separation of Fe–Fe atoms within the dimmers, probably preventing the establishment of a FM coupling in the Fe sublattice, as commented above, and (iii) the strong variation of the Mn–Mn distances along the chains of $Mn^{4+}O_6$ octahedra, which probably hinder the consolidation of a FM coupling for each whole chain, opposite to what happens in other RMnFeO$_5$ oxides. It is clear that there are competing interactions that drive the divergence of the ZFC vs. FC susceptibility curves, indicative of magnetic disordering and a certain spin frustration that prevent the consolidation of a long-range ferrimagnetic structure. The absence of long-range magnetic ordering observed for BiFeMnO$_5$ from NPD data confirms this hypothesis.

5. Conclusions

Two new compounds of formula $BiFe_xMn_{2-x}O_5$ (x=0.5, 1.0) have been obtained by partially replacing Mn by Fe in the parent $BiMn_2O_5$ oxide. Their crystallographic structures are isotypical with that of RMn_2O_5 materials (space group Pbam), and contains chains of edge-linked $Mn^{4+}O_6$ octahedra connected by dimer groups of square pyramids $(Fe,Mn)^{3+}O_5$. Most of the Fe atoms are introduced over the pyramidal positions as Fe^{3+}, however, a certain degree of disorder is observed in both samples implying that also some Fe cations are introduced in the octahedral position. The presence of the electronic lone pair on Bi^{3+} severely distorts the crystal structure. The $(Fe,Mn)^{3+}O_5$ square pyramids are flattened with respect to $BiMn_2O_5$; the Fe–Fe separation within the dimers of pyramidal units and the Mn–Mn distances along the chains of octahedra significantly vary with x, weakening the intra-dimer magnetic interactions and the FM coupling along the chains and, therefore, preventing the establishment of a long-range ferrimagnetic structure, as observed in all the other RFeMnO$_5$ isotypical oxides.

Acknowledgments

We acknowledge the financial support of the Spanish Ministry of Education to the project MAT2010-16404. We are grateful to Dr. M. García-Hernández for performing the magnetic measurements. We thank the ILL, Grenoble (France), for making the neutron beam time available. We are also grateful for the CSIC-BAS project P2007BG0013.

References

[1] W. Eerenstein, N.D. Mathur, J.F. Scott, Nature 442 (2006) 759–765.
[2] R. Ramesh, N.A. Spaldin, Nat. Mater. 6 (2007) 21–29.
[3] H. Tsujino, Y. Tanaka, K. Kohn, In: M. Abe and T. Yamaguchi (Eds.). Proceedings of the 6th International Conference on Ferrites (Tokyo and Kyoto); 1992.
[4] K. Saito, K. Kohn, J. Phys.: Condens. Matter 7 (1995) 2855–2863.
[5] A. Inomata, K. Kohn, J. Phys.: Condens. Matter 8 (1996) 2673–2678.
[6] Y.F. Popov, A.M. Kadomtseva, S.S. Krotov, G.P. Vorob'ev, M.M. Lukina, Ferroelectrics 279 (2002) 147–156.
[7] Y.F. Popov, A.M. Kadomtseva, S.S. Krotov, G.P. Vorob'ev, M.M. Lukina, M.M. Tegranchi, J. Exp. Theor. Phys. 96 (2003) 961–965.
[8] S. Quezel-Ambrunaz, E.F. Bertaut, G. Buisson, C.R. Acad. Sci 258 (1964) 3025–3028.
[9] E.F. Bertaut, G. Buisson, A. Durif, A. Mareschal, M.C. Montmory, S. Quezel-Ambrunaz, Bull. Soc. Chim. Fr. (1965) 1132–1137.
[10] J.A. Alonso, M.T. Casais, M.J. Martínez-Lope, I. Rasines, J. Solid State Chem. 129 (1997) 105–112.
[11] J.A. Alonso, M.T. Casais, M.J. Martínez-Lope, J.L. Martinez, M.T. Fernández-Diaz, J. Phys.: Condens. Matter 9 (1997) 8515–8526.
[12] A. Muñoz, J.A. Alonso, M.J. Martínez-Lope, J.L. Martínez, Chem. Mater. 16 (2004) 4087–4094.
[13] M. Retuerto, M.J. Martínez-Lope, A. Muñoz, T. Ruskov, I. Spirov, K. Krezhov, M.T. Fernández-Díaz, M. García-Hernández, J.A. Alonso, Solid State Commun. 150 (2010) 1831–1836.
[14] M.J. Martínez-Lope, M. Retuerto, J.A. Alonso, V. Pomjakushin, J. Solid State Chem. 181 (9) (2008) 2155–2160.
[15] A. Muñoz, J.A. Alonso, M.J. Martínez-Lope, J.L. Martínez, Eur. J. Inorg. Chem. (2007) 1972–1979.
[16] A. Muñoz, J.A. Alonso, M.J. Martínez-Lope, J.L. Martínez, Phys. Rev. B 72 (2005) 184402-8.
[17] M.J. Martínez-Lope, M. Retuerto, J.A. Alonso, M. García-Hernández, K. Krezhov, I. Spirov, T. Ruskov, M.T. Fernández-Díaz, Solid State Commun. 149 (2009) 540–545.
[18] A. Muñoz, J.A. Alonso, M.T. Casais, M.J. Martinez-Lope, J.L. Martinez, M.T. Fernández-Diaz, Phys. Rev. B 65 (2002) 144423-8.
[19] K. Masuno, Nippon Kagaku Zasshi 88 (1967) 726–730.
[20] C.M. Jiménez, Bol. Soc. Esp. Ceram. Vidrio 17 (1978) 365.
[21] D.M. Giaquinta, H.C. zur Loye, J. Alloys Compd. 184 (1992) 151–160.
[22] H.M. Rietveld, J. Appl. Crystallogr. 2 (1969) 65–71.
[23] J. Rodriguez-Carvajal, J. Phys. B 192 (1993) 55–69.
[24] M.J. Martínez-Lope, J.A. Alonso, unpublished results.
[25] R.D. Shanon, Acta Crystallogr. Sect. A 32 (1976) 751–767.